ZIBELINE INTERNATIONAL PUBLISHING

ISSN: 2521-5035 (Print)
ISSN: 2521-5043 (online)

Earth Sciences Malaysia (ESMY)

DOI : http://doi.org/10.26480/esmy.01.2018.16.21

CODEN : ESMACU

IMPROVED MAGNETIC DATA ANALYSES AND ENHANCEMENT TECHNIQUES FOR LITHOLOGICAL AND STRUCTURAL MAPPING AROUND AKURE, SOUTHWESTERN NIGERIA

Akingboye A. Sunny*, Ademila Omowumi, Ogunyele A. Chris

Department of Earth Sciences, Adekunle Ajasin University, Akungba-Akoko, PMB 001, Ondo State, Nigeria
****Corresponding Author Email: adedibu.akingboye@aaua.edu.ng***

ARTICLE DETAILS

Article History:

Received 12 November 2017
Accepted 12 December 2017
Available online 1 January 2018

ABSTRACT

This study employs improved magnetic data analyses and enhancement techniques to map and interpret the lithological and structural features around Akure and its environs. Several forms of filtering processes were performed to improve and enhance the Total Magnetic Intensity (TMI) data and other reduced data that were later produced. The analysed results of the upward continuation to 500 *m* and 1 *km* revealed the attitudes of deep-seated basement rocks and anomalous structures with regional trend of NW-SE direction, as well as depth of structures that ranged beyond 1 km. On the other hand, derivatives images revealed lineaments/faults: F1-F'1, F2-F'2, F3-F'3 (minors) and F4-F'4 trending NNE-SSW, N-S, NE-SW, minor (ENE-WSW and E-W) and NW-SE respectively. Based on magnetisation contrast, four amplitude zones were revealed on the Analytic Signal (AS) image, which include very high zone as migmatite complexes; intermediate zone as migmatite/gneiss and charnockite complexes; fairly low zone as granite-gneiss and granite complexes, and low zone as quartzite ridge/ complex. The large causative bodies delineated from the pseudo-gravity revealed density of about 0.133 g/cc in susceptibility. The total depth estimate to top of magnetic sources ranged from 53 *m* to 1.98 *km* for shallower and deeper sources respectively. This study, therefore, suggests different rock types of varying mineralogical compositions, tectonic framework and structural deformations that led to change in intensity of rocks in the study area.

KEYWORDS

Automatic Gain Control (AGC), Analytic Signal (AS), Pseudo-gravity, Spectral plot, Litho-structure, Akure.

1. INTRODUCTION

Magnetic method is one of the potential field methods that exploits the considerable difference in the variation in geomagnetic field due to variations in percentages of magnetite and other magnetic minerals that give magnetic field signatures, chemical inhomogeneities, depositional and/or crystallization conditions and post deformational conditions. It reflects the variation in the distribution and type of magnetic minerals in the subsurface. Magnetic minerals can be mapped from the surface to greater depth in crustal rocks depending on dimension, shape, and the magnetic property of the rock. Sedimentary formations do not usually have appreciable magnetic properties because of the minute contribution of detrital remnant magnetism while igneous and metamorphic rocks exhibit greater variations [1, 2].

This method has been used by some authors either as a single method or in combination with other geophysical methods in parts of the study area (Akure) as regard to data reductions, data enhancement and interpretations for various applications. Magnetic data require proper filtering processing through various filters application in order to accentuate important diagnostic features (anomalies), if much information must be drawn from the dataset for both qualitative and quantitative interpretations.

Magnetic method is a useful tool in groundwater investigation, mineral and hydrocarbon explorations, as well as environmental/pollution study through detailed interpretation of the total field magnetic; by mapping of subsurface basement structures and lithology, delineating boundaries and edges of magnetizing bodies, basement modelling (profile/ configuration) and depth to top of magnetic sources.

Therefore, this study is aimed at mapping and interpreting the lithological and structural features around Akure and its environs. The results and conclusion drawn from this study would serve as guides for geologically related decision making prior to mineral exploration, groundwater, environmental and engineering investigations in Akure metropolis and its environs.

2. LOCATION AND GEOLOGIC SETTING

Aeromagnetic dataset of Akure Sheet 264 is used as the study area for this work. It lies between Latitude 7° 00' and 7° 30' N (770000 - 830000 *m*N) and Longitude 5° 00' and 5° 30' E (720000 – 777500 *m*E) of Zone 31N Greenwich Mercator (Figures. 1 and 3). The towns in the study area include Akure metropolis (Akure North and Akure South), Shasha, Ogbesi, Ikere-Ekiti and some parts of Ado-Ekiti. The areas are accessible mainly by roads and foot paths.

The study area falls within the Basement Complex of Southwestern Nigeria (Figure 1). The Basement Complex rocks of Nigeria forms a part of the African Crystalline Shield which occurs within the Pan-African Mobile Belt that lies between the West African and Congo Cratons and South of the Tuareg Shield which were affected by the Pan-African Orogeny. The Southwestern besement is within the triangular portion of the Nigerian besement, an extension of the Dahomeyide Shield of the West African Craton. Rocks of the region include Migmatized-Gneiss Complex (MGC) that is characterized by a) grey foliated gneiss, b) ultramafic rocks and c) felsic component comprised of pegmatite, aplite and granitic rocks [3, 4].

The MGC in Southwestern Nigeria is affected by three major geotectonic events ranging from Early Proterozoic of 2000 Ma to Pan-African events of ~600 Ma [5-7]. The rocks of the basement have been affected by medium pressure Barrovian metamorphism [7, 8]. The number of outcrops varies considerably from one area to another which is accounted for partly by differing resistance to weathering presented by the various

rock types; homogenous and massive rocks being less likely to be weathered than the others [9].

The general geology of the study area is well researched in the works of other researchers [7, 10, 11]. Akure is underlain by Precambrian rocks typical of the Basement Complex of Southwestern Nigeria, comprising of these major lithological units: migmatites, granodiorite, granites, charnockites, granite gneiss, quartzite and other felsic and mafic intrusives. The Basement rocks show great variations in grain size and in mineral composition.

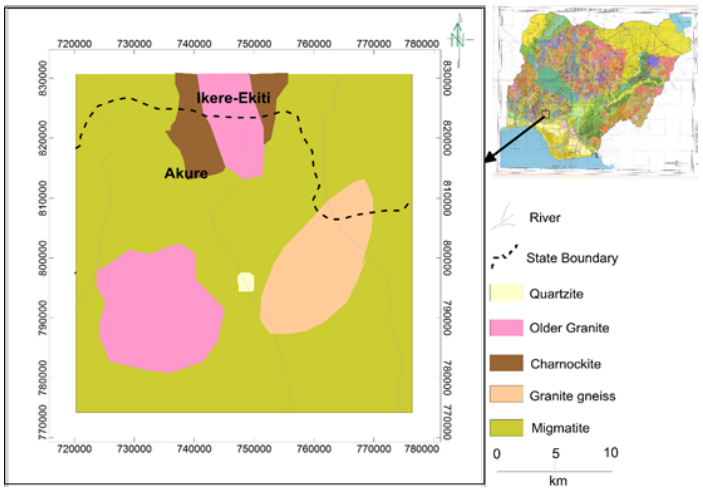

Figure 1: Geological Map of the Study Area (modified after [12])

3. MATERIAL AND METHODS

Aeromagnetic data of Akure Sheet 244 (1:100 000) was acquired from Nigerian Geological Survey Agency (NGSA) and processed using Geosoft® Oasis Montaj™ software, other software include; Surfer and Microsoft Excel.

Data reductions such as: removal of near surface noise (NSN), reduction to magnetic equator, regional field, residual field, automatic gain control (AGC), upward continuation, tilt-angle derivative (TDR), second vertical derivative (SVD), analytic signal (AS), pseudo-gravity, radial average power spectrum (RAPS)/spectral plot were performed for better result output.

The data reductions and enhancements were done using the MAGMAP Step-by-Step filtering processing. The Magnetic data processing flow chat in Figure 2 shows the data processing stages employed.

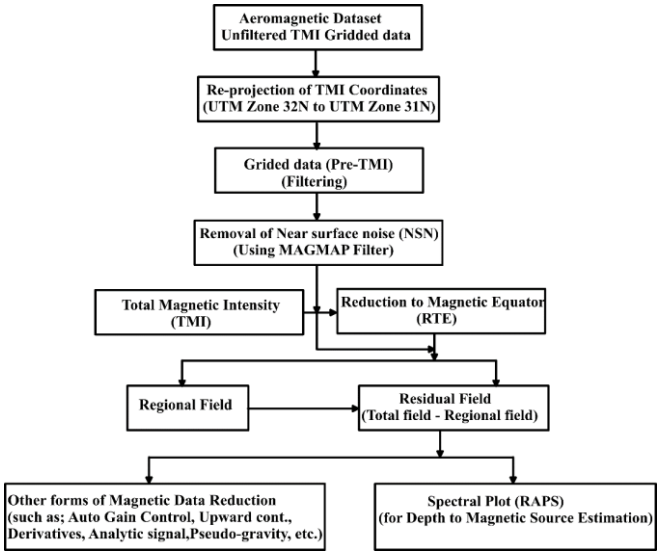

Figure 2: Data Processing Flow Chat

3.1 Re-projection of Coordinates and Near Surface Noises (NSN) Removal

The NGSA Total Magnetic Intensity (TMI) data coordinates were re-projected from UTM Zone 32N to UTM Zone 31N of the Greenwich Mercator. This was necessary because the coordinates of the data must correspond to their actual locations. These re-projected data were gridded and adopted as the new TMI data and was filtered to remove Near Surface Noises (NSN) caused by metallic materials, fences, cables (both buried and surface), flight height, etc.

3.2 Reduction to Magnetic Equator (RTE)

The Reduction to Magnetic Equator (RTE) filter was used to produce the RTE_TMI image, in order to Centre structures and anomalous bodies over their exact positions. To produce anomalies, depend on the inclination and declination of the body's magnetization, inclination, and declination of the local earth's field and orientation of the body with respect to the magnetic north [13]. As discussed in a study, problems can arise in the reduction to the pole process at magnetic latitudes less than 15°, as the Fourier domain transformation process becomes unstable, owing to the need to divide the spectrum by a very small term, thereby introducing north–south alignment of the anomalies into the data [14]. The RTE_TMI gridded data (Figure 3) was adopted as our new processed data for subsequent data analyses and enhancement.

3.3 Regional and Residual Fields

The Regional Field associated with deep masses were filtered out to produce the Residual data for the area covered. The data were smoothed upward to 4km to evince the regional field caused by deep basement rocks and high wavelength anomalies. The Residual data left after near surface noise and the regional have been removed is produced using equation 1:

$$\textbf{\textit{Residual field}} = Observed\ Total\ field\ (RTE\_TMI) - Regional\ field \qquad (1)$$

3.4 Automatic Gain Control (AGC)

Automatic Gain Control (AGC) is used to accentuate coherent assemblages and to align anomalies that appear characterless in RTE_TMI image by accentuating equal signals with both low and high amplitudes anomalies that mapped out the structures in the areas. Thus, the filter makes smaller trends and fractures to be distinct and clearly seen by unaided eyes [15-17].

3.5 Upward Continuations

Upward Continuation is considered a clean filter because it produces almost no side effects that may require the application of other filters or processes to correct. Because of this, it is often used to remove or minimize the effects of shallow sources and noise in grids. Also, upward continued data may be interpreted numerically and with modeling programs. This is not the case for many other filter processes. Upward continuation was carried out on the RTE_TMI data to depth of 0.5 km (500 m) and 1 km respectively. Equation2 below can be used for the calculation of the upward continuation [18].

$$F(x,y,-h) = \frac{h}{2\pi}\iint \frac{F(x,y,0)\partial x\partial y}{\{(x-x')^2+(y-y')^2+h^2\}^{1/2}} \qquad (2)$$

Where; $F\ (x',y',-h)$is the total field at the point $P\ (x',y',-h)$above the surface on which $F\ (x',y',0))$ is known, h is the elevation above ground surface.

3.6 Second Vertical Derivative (SVD)

The significance of vertical and horizontal derivatives in locating the position of the density or magnetization boundaries were given in the works of a few researcher [2,19].

The RTE_TMI image contains all the anomalies both shallow and deep sources. Therefore, second vertical derivatives (SVD) filtering was used to suppress unwanted sources (and accentuates some) that were obscured by broader regional trend. In this case, it accentuates short wavelength components of the field and de-emphasizing the long wavelength components to sharpen the edges of the anomalies; tends to reduce anomaly complexity and allow clearer contrast between the geologic unit sand causative structures like lineaments/faults and smaller trends.

3.7 Tilt-angle Derivative (TDR)

The Tilt Derivative (TDR) is produced from the tilt derivative filter. It is used to determine structures, trends, contacts and edges or boundaries of magnetic sources, as well as to enhance both weak and strong magnetic anomalies of the area by placing an anomaly directly over its source, especially at shallow depths by using the theory that the zero contours are the edges of the formation [20].

Mathematically, the equations below were used to calculate the tilt-angle and tilt horizontal derivatives respectively, the units for both are in radians:

$$HD\_TDR = \sqrt{\left(\left(\frac{dT}{dx}\right) + \left(\frac{dT}{dy}\right)\right)} \quad (3a)$$

$$TDR = \arctan\left(\frac{1VDT}{HD\_TDR}\right) \quad (3b)$$

where, 1VDT is the first vertical derivative in z-direction, dT/dx is the derivative in x-direction, and dT/dy is the derivative in y- direction

3.8 Analytic Signal (AS)

Analytic Signal (AS) or total gradient is formed through the combination of the horizontal and vertical gradients of the magnetic anomaly and it is applied either in space or frequency domain, generating a maximum directly over discrete bodies as well as their edges. The generated maximum directly over the causative body and depth estimation abilities of this filter make it a highly useful technique for magnetic data interpretation. The maximum can be used to detect the structures responsible for the observed magnetic anomalies over an area [21-23]. Analytic signal images are useful as a type of reduction to the pole, as they are not subjected to the instability that occurs in transformations of magnetic fields from low magnetic latitudes [14]; source positions regardless of any remanence in the sources [17].

The amplitude A of the analytic signal (AS) of the total magnetic field F is calculated from the two or three orthogonal derivatives of the field for 2D or 3D bodies respectively (equation 4). It is therefore defined as the square root of the squared sum of the vertical and horizontal derivatives of the magnetic field [22, 24]:

$$|A(x,y)| = \sqrt{\left(\frac{\partial F}{\partial x}\right)^2 + \left(\frac{\partial F}{\partial y}\right)^2 + \left(\frac{\partial F}{\partial z}\right)^2} \quad (4)$$

$|A(x,y)|$is the analytic signal amplitude and $F$is the observed magnetic field at (x, y).

3.9 Pseudo-gravity

Pseudo-gravity filter enhances the anomalies associated with deep magnetic sources at the expense of the dominating shallow magnetic sources. This can be used for detection of deep, magnetic igneous plutons and volcanic piles. It is a suitable tool for interpreting deep-seated mineral plumbing systems associated with known, shallow mineral occurrences [25].

Therefore, the pseudo gravity can be produced by using equation 5 (Oasis Montaj™ help file):

$$\mathrm{L}(\theta) = \frac{G*d/J}{[\sin(I_a)+i\cos(I)*\cos(D-\theta)]^2*r}, if\ ((I_a) < (I)), I_a = I \quad (5)$$

*where, I = geomagnetic inclination, I = inclination for amplitude correction, d = density contrast (g/cm^3), g = gravitational constant (6.67*10^{-8}), J = magnetisation in guass , D = geomagnetic declination, θ=direction of wavenumber, and r = wavenumber (radians/ground)=2πk*

The pseudo-gravity data can be modelled using conventional map and inversion methods, where the density is considered as a pseudo-density defined by the relationship [25]:

$$D=kH/\gamma \quad (6)$$

Where D is the density contrast, k is magnetic susceptibility, H is the total magnetic field intensity, and γ is the universal gravitational constant. This relationship assumes that the magnetization is induced and no remanence is present.

3.10 Radially Averaged Power Spectrum (RAPS)

Radially Averaged Power Spectrum (RAPS) which is also known as spectral plot was run for depth to top of magnetic sources estimations. The frequency unit is in radians per kilometer (rad/km), the mean depth of burial of the ensemble is given by equation 6 (Oasis Montaj ™ help file):

$$Z = -\frac{m}{4\pi} \quad (7)$$

Therefore, various maps produced through reductions and enhancements were qualitatively and quantitatively interpreted.

4. RESULTS AND DISCUSSION

The RTE_TMI image (Figure 3) evinced positive magnetic intensity value as high as 532.35 nT which dominated almost half of the entire area, covering the central to the eastern, northeastern and very small segment of the northwestern parts of the study area. The southwestern and western parts of the study area are obviously dominated by low magnetic intensity (negative values) which ranged between -418.29 to -6.64 nT. These variations are results of different mineral compositions, tectonic framework and structural features that are the major contributors to difference in magnetic intensities observed in the entire area.

On the other hand, the Residual image (Figure 4) reveals clearer shallow anomalies which could not be easily mapped out in Figure 3 after the effect of deep-seated anomalies had been removed. The areas delineated as A and B, are places in the study area where basement rocks could be outcropping or close to the surface, but D and C are likely edges/boundaries of magnetizing bodies. The rocks in these areas are highly deformed and some parts evince fractures (F – F') as we traversed left of the mapped-out section of the image (in white color). On the right hand of this line, there is a possibility of having rocks that are different from those on the left because of their unique setting in terms of deformation (fracturing, shearing, etc.) and uniformity in magnetic intensity values.

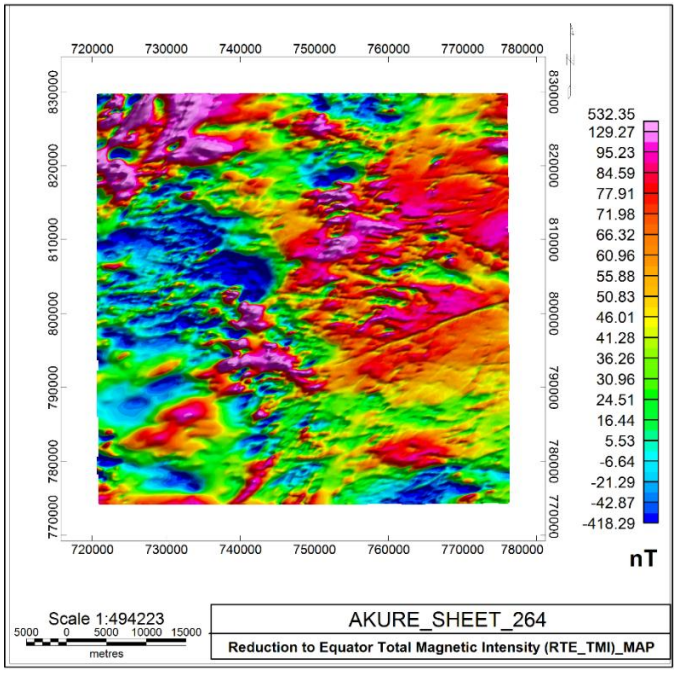

Figure 3: Colour Shaded Reduction to Equator Total Magnetic Intensity (RTE_TMI) Image.

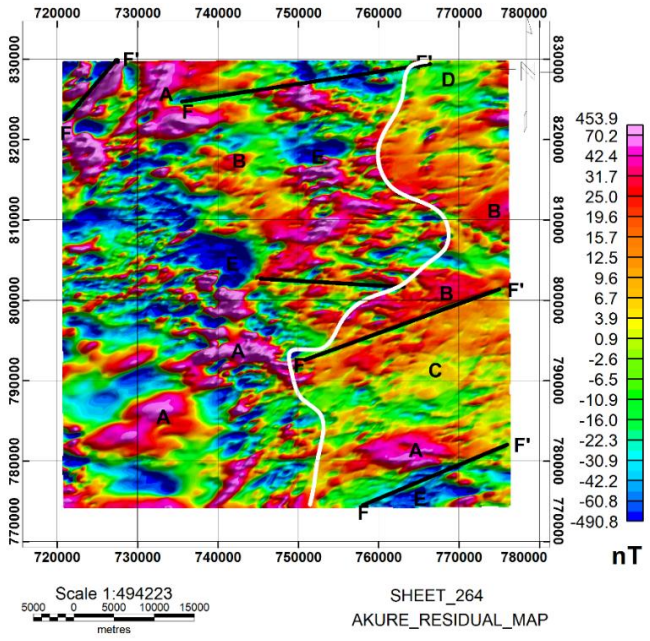

Figure 4: Residual Image produced after the removal of the Regional Field from Total Observed Field (RTE_TMI).

In Figure 5, the Automatic Gain Control (AGC) image gives a robust viewof coherent assemblages and well aligned anomalous structures, especially smaller trends within; with positive intensity signals that ranged from 63 - 769 nT and -974.1 to -16.2 nT for negative anomalies.

Figures 6a and 6b show the images of the upward continued RTE_TMI gridded data to 500 *m* (0.5 *km*) and 1 *km* respectively, basically to infer the attitudes of basement structures with depth. The positive anomaly evinced by these images at the extreme end of the northwestern part, from the central to eastern and to the northeastern part are deep-seated basement rocks with high magnetic mineral constituents and crystallized lattices framework. On the contrary, the negative anomalous zones at the western to some part of the southern axes have structures that are pronounced and seen beyond 0.5 *km*. These structures diminish as the depth of continuation increases to 1 *km*. The upward continued images revealed that the regional trend of the rocks in the study area is in NW-SE direction, as distinctively seen in Figure 6b.

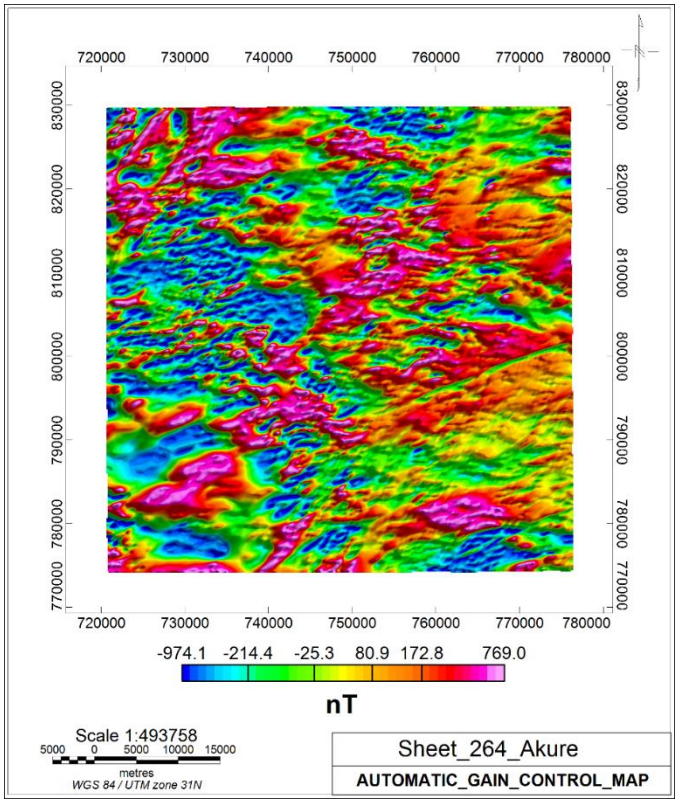

Figure 5: Automatic Gain Control (AGC) Image

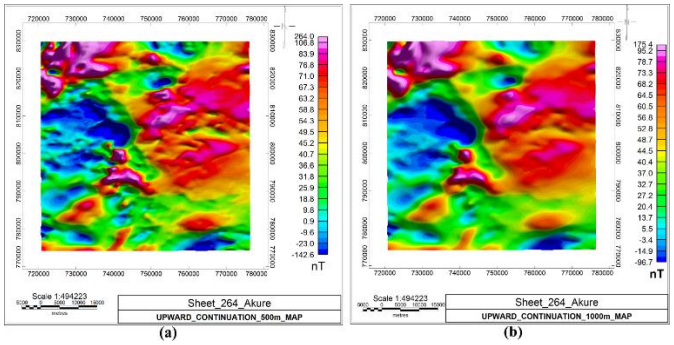

Figures 6: Upward continued RTE_TMI Images; (a) 500 *m*, and (b) 1 *km*

The Second Vertical Derivative (SVD) (Figure 7) sharpens the edges of magnetic anomalies, gives clearer contrast between the geologic unit sand causative structures such as lineaments/faults and smaller trends in the area.

Prominent lithologic contacts observed are: the migmatite complexes (marked as A and delineated in red lines) boundaries with other basement rocks. Points B, C, D, and E highlight areas occupied by granite-gneiss, granite, charnockite and quartzite complexes respectively. Areas with the question marks and blue polygonal shape are other suspected rocks that were not shown on the geological map. The migmatite complexes evinced highly deformed and characterless structures and their boundaries are well defined when compared with other complexes in the area. Some structural lineaments (faults) are highlighted in green colours with varying trending directions.

The Tilt Derivative (TDR) (Figure 8) accentuates structural deformations such as faults, joints, and arched zones or even geological contacts. Magnetic minerals are mainly concentrated along or aligned with some structures. TDR image displays most structural feature of the study area such as the inferred faults, contacts and to some extent the shape of some lithologic. The lineaments/faults are marked in red ticks while lithological trends are seen in varying trends and arched curves. Four (4) lineament (faults and joints) systems were identified on this images by observing the abrupt changes between the positive and negative magnetic anomalies. The lineament systems are: F1-F'1, F2-F'2, F3-F'3 (minors) and F4-F'4 trending NNE-SSW (including approximately N-S trend), NE-SW, minor (ENE-WSW and E-W) and NW-SE respectively.

The basement rocks are seen to be highly fractured, deformed and it is believed that some of these rocks have undergone more than one episode of orogeny. The lithologic contact observed are the edges mapped out where there are changes in the signatures of lithologies, as seen towards the extreme end of the southwestern part of the image, occupied by granitic rocks and magmatite, hence, this further prove the originality of the geological map, because of less features envisaged on them.

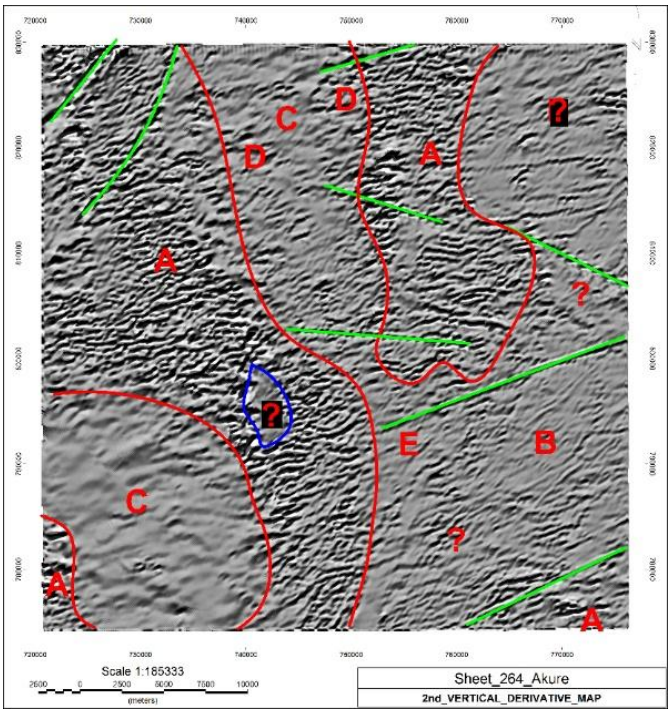

Figure 7: Grey Second Vertical Derivative (SVD) Image.

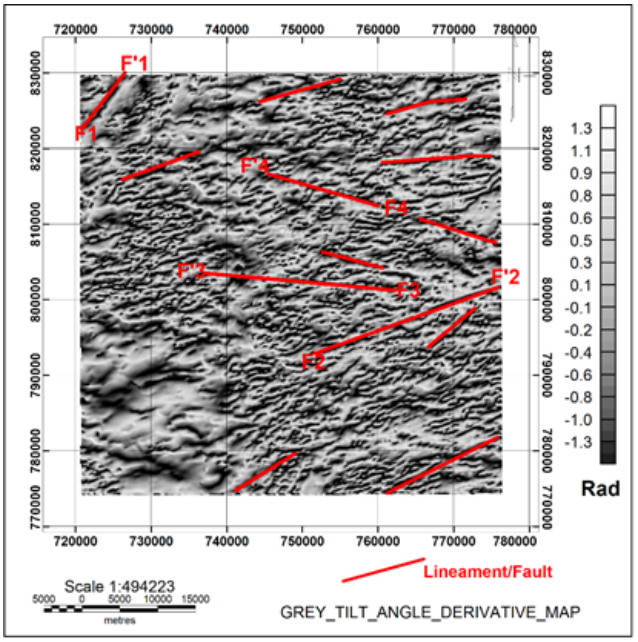

Figure 8: Tilt Derivative (TDR) Image.

The Analytic Signal (AS) image (Figure 9) centers the peak of the magnetising bodies symmetrically over their sources through transformation of the shapes of inclined magnetising bodies. It also accentuates the variation in the magnetization of the magnetic sources and highlights discontinuity and anomaly textures. On comparison with Figure 7 (SVD image), both images evince similar anomaly pattern, in terms of structural trends, edges of anomalous sources, and lithological contacts based on the magnetisation of various rock compositions. According to some researchers, high amplitude magnetic anomalous zones are associated with high magnetisation contrast in rocks [14, 26]. Therefore, Figure 9 evinced four (4) different magnetic analytic signal zones, which include:

1. high amplitude magnetic zone defined as edges and trends of the migmatite (M) complexes;
2. intermediate amplitude magnetic zone as edges, trend and magnetisation strength of areas consisting migmatite/gneiss (M/Ggn), and charnockite (Ch) complexes;
3. fairly low amplitude magnetic zone as areas occupied by granite-gneiss (Ggn) and granite (G) complexes, and
4. low amplitude magnetic zone delineated as edges of the quartzite (Qz) ridge/complex. However, low amplitude signals are seen within some rock bodies, probably due to low magnetisation response of the source generating this signal.

The migmatite-gneiss complexes were initially granite-gneiss complexes but were further metamorphosed to their present form leaving wide area extent of granite-gneiss complex in the southeastern part of the area.

Similarly, when compared with Figure 8, it is also noted that migmatite and gneiss complexes have been intruded by a quantum number of minor intrusive rocks (veins, dykes, sills, etc). Figure 9 shows that the rocks trend NW-SE direction while the quartz veins are the low amplitude trends.

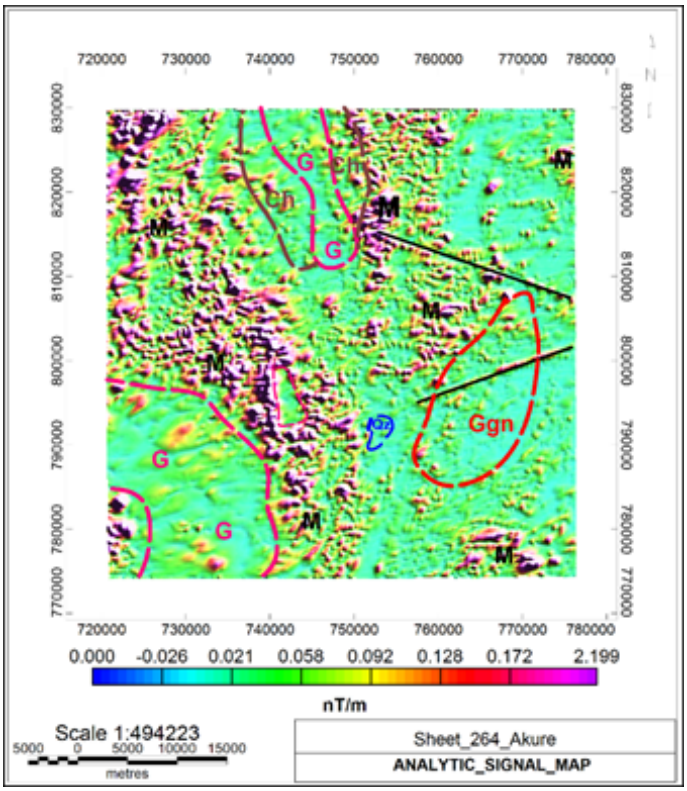

Figure 9: Analytic Signal (AS) Image produced to rshow the litho-structures and trends in the study area

**M-Migmatite, Ggn-Granite Gneiss, Qz-Quartzite, G-Granite, Ch-Charnockite*

According to Blakely [27], in other studies, to locate and outline crustal magnetic sources, pseudo-gravity transformation becomes very useful in such magnetic anomalies interpretation. Therefore, Figure 10 shows the accentuated pseudo-gravity anomalies from deep magnetic sources that are associated with deep basement rocks and causative bodies.

The pseudo-gravity transformation is done at Inclination of -10 and declination of -1.

The pseudo-gravity technique is useful in deep-seated anomalies mapping because gravity anomalies are in some ways more instructive and easier to interpret and quantify than magnetic anomalies. When the pseudo-gravity image (Figure 10) is compared to Figures 4, 7 and 9, the area of high density coincides with the migmatitic and granite-gneissic rocks which are older than other rocks in the area. It is also in agreement with Figure 6 (upward continuation images) having deduced a large causative body trending NW-SE with a density of about 0.133 g/cc in susceptibility.

Radially Averaged Power Spectrum (RAPS) or Spectral plot (Figure 11) reveals the total depth estimate to the top of magnetic sources that produced the observed anomalies in the study area using spectral analysis. The gradient of the layers was calculated based on the wavelength of the magnetic sources. The gradient of the shallower and deeper magnetic sources is 0.67 and 24.89 respectively. Therefore, the total depth estimate to the top of magnetic shallower and deeper sources in the area are 53 m and 1.98 km respectively.

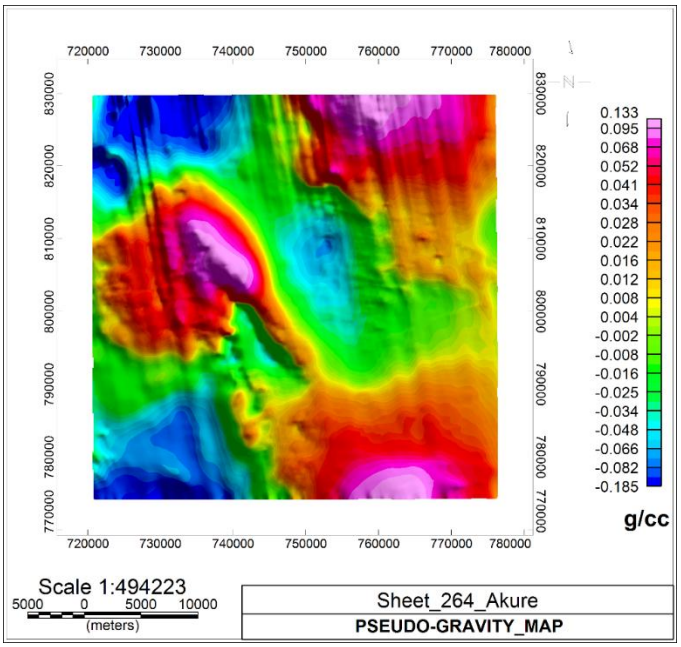

Figure 10: Colour Shaded Pseudo-Gravity Image

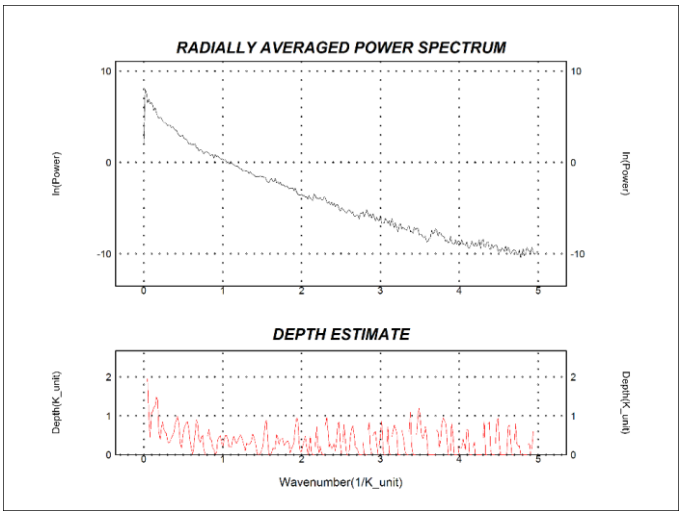

Figure 11: Radially Averaged Power Spectrum (RAPS)/Spectral plot.

5. CONCLUSION

In this study, aeromagnetic mapping through improved magnetic data analyses and enhancement techniques was carried out to reveal the lithologies, structures such as lineaments/faults, trends, and other zones of weaknesses, as well as sharp contacts within the rocks around Akure. These features were revealed through different range of magnetic intensity values that suggest different rock types of varying mineralogical

compositions, tectonic framework and structural deformities.

The upward continuations, Second Vertical Derivatives (SVD) and Tilt Derivatives (TDR) reveal the rock contacts, structures and trends. The delineated structures (lineaments/faults) strike N-S, NE-SW, NW-SE, NNE-SSW, ENE-WSW and E-W generally in accordance with the major structural trend of the Basement Complex of Nigeria as observed from earlier works by [28-32]. Furthermore, the Analytic Signal (AS) image have proven the robustness of this technique in geological mapping by categorising different litho-structures basically on their mignetisation contrast, as well as reveal the lithostructural trends.

On the pseudo-gravity image, high density areas coincide with the migmatitic and granite-gneissic rocks which are older than other rocks such as quartzite,, charnockites, granite sand other minor intrusives in the area. The total depth estimation to the top of magnetic sources for the study area as shown on the spectral plot ranged from 53 *m* to 1.98 *km* for shallower and deeper sources respectively.

This study, therefore, reveals that the migmatite-gneiss complexes were initially granite-gneiss complexes, but were later metamorphosed to their present state leaving a wide area extent of granite-gneiss complex around the southeastern part of the study area. Similarly, it is also noted that the migmatitic rocks have been intruded by a quantum number of intrusives such as veins, dykes, sills, etc.

REFERENCES

[1] Jayeoba, A., Odumade, D. 2015. Geological and structural interpretation of Ado-Ekiti and its adjoining areas using aeromagnetic data. Adapted from extended abstract prepared in conjunction with oral presentation given at Pacific Section AAPG, SEG and SEPM Joint Technical Conference, Oxnard, California. Search and Discovery article, 1-32.

[2] Okpoli, C., Akingboye, A. 2016. Reconstruction and appraisal of Akunu–Akoko area iron ore deposits using geological and magnetic approaches. RMZ – Materials and Geo Environment Journal, 63, 19-38.

[3] Oyawoye, M.O. 1972. The Basement complex of Nigeria. In: In: African Geology, edited by Dessauvagie T. F. J. and Whiteman A. J. University of Ibadan, 66-102.

[4] Rahaman, M.A. 1981. Recent Advances in the Study of the Basement Complex of Nigeria. First Symposium on the Precambrian Geology of Nigeria, Summary.

[5] Woakes, M., Ajibade, C. A., Rahaman, M.A. 1987. Some metallogenic features of the Nigerian Basement. Journal of Africa Science, 5, 655-664.

[6] Ajibade, A. C., Fitches W. R. 1988. The Nigerian Precambrian and the Pan–African Orogeny, Precambrian Geology of Nigeria, 45-53.

[7] Oyinloye, A.O. 2011. Geology and Geotectonic Setting of the Basement Complex Rocks in Southwestern Nigeria: Implications on Provenance and Evolution. Earth and Environmental Sciences, 98 – 117.

[8] Rahaman, M.A., Emofureta, W.O., Vachette, M. 1983. The potassic-grades of the Igbeti area: Further evaluation of the polycyclic evolution of the Pan-African Belt in Southwestern Nigeria. Precambrian Research, 22, 75-92.

[9] Jones, H.A., Hockey, 1964. The Geology of part of' Southwestern Nigeria. Geological Survey, Nigeria bulletin, 31.

[10] Rahaman, M.A. 1976. Review of Basement Geology of Southwestern Nigeria. In: Kogbe, C.A., (edn.) Geology of Nigeria. Rock View (Nig.) Limited, Jos, Nigeria, 39-56.

[11] Ademilua, O. L. 1997. A Geoelectric and Geologic Evaluation of Groundwater Potential of Ekiti and Ondo States, Southwestern Nigeria, Unpublished M.Sc. Thesis, Department of Geology, Obafemi Awolowo University, Ile-Ife, Nigeria, 1-67.

[12] Geological Map of Nigeria. 2004. Nigerian Geological Survey Agency (NGSA), Garki, Abuja.

[13] Baranov, V. 1957. A New Method for Interpretation of Aeromagnetic Maps Pseudo-Gravimetric Anomalies. Geophysics, 22, 359-383.

[14] MacLeod, I.N., Jones, K., Dai, T.F. 1993. 3-D analytic signal in the interpretation of total magnetic field data at low magnetic latitudes. Exploration Geophysics, 24, 679-688.

[15] Rajagopalan, S. 1987. The use of automatic gain control to display vertical magnetic gradient data. Exploration Geophysics, 18, 166-169.

[16] Rajagopalan, S., Milligan, P. 1995. Image enhancement of aeromagnetic data using automatic gain control. Exploration Geophysics, 25, 173-178.

[17] Milligan, P.R., Gunn, P.J. 1997. Enhancement and presentation of airborne geophysical data. AGSO Journal of Geology and Geophysics, 17, 63-75.

[18] Telford, W.M., Geldart, L.P., Sheriff, R.E., Keys, D.A. 1990. Applied Geophysics. Cambridge University Press. 744.

[19] Cordell, L., Grauch, V.J.S. 1985. Mapping basement magnetization zones from aeromagnetic data in the San Juan basin, New Mexico, in The Utility of Regional Gravity and Magnetic Anomaly Maps, edited by W. J. HINZE. Society of Exploration Geophysics, 181-197.

[20] Salem, A., Williams, S., Fairhead, J., Ravat, D., Smith, R. 2007. Tilt-depth method: a simple depth estimation method using first-order magnetic derivatives. The Leading Edge, 26, 1502-1505.

[21] Nabighian, M.N. 1984. Toward a three-dimensional automatic interpretation of potential field data via generalized Hilbert transforms: fundamental relations. Geophysics, 49, 780-786.

[22] Roest, W.R., Verhoef, J., Pilkington, M. 1992. Magnetic interpretation using the 3D analytic signal.Geophysics, 57, 116-125.

[23] Ansari, A.H., Alamdar, K. 2009. Reduction to the Pole of Magnetic Anomalies Using Analytic Signal. World Applied Sciences Journal, 7 (4), 405-409.

[24] Nabighian, M.N. 1972. The analytic signal of two-dimensional magnetic bodies with polygonal cross-section: Its properties and use for automated anomaly interpretation. Geophysics, 37, 501–517.

[25] Pratt, D.A., Shi, Z. 2004. An Improved Pseudo-Gravity Magnetic Transform Technique for Investigation of Deep Magnetic Source Rocks: ASEG 17th Geophysical Conference and Exhibition, Sydney, 1-4.

[26] Macleod, I. A., Vieira, S., Chaves, A. C. 1993. Analytic Signal and Reduction-to the-Pole in the interpretation of Total Magnetic Field Data at Low Magnetic Latitudes.3rd Conference of the Brazillian Geophysical. Society. pp. 831-835.

[27] Blakely, R.J. 1995. Potential Theory in Gravity and Magnetic Applications. Cambridge University Press, Cambridge, 441.

[28] Ako, B.D., Ojo, S.B., Okereke, C.S., Fieerge, F.C., Ajayi, T.R., Adepelumi, A.A., Afolayan, J.F., Afolabi, O., Ogunwusi, H.O. 2004. Some Observations from Gravity/Magnetic Data Interpretation of the Niger Delta: NAPE bulletin, 17, 11-21.

[29] Babafemi, E.M., Bamidele, O.E., Sangodiji, E.E. 2016. Mapping of Structural Features in Basement Complex Part of Southwestern Nigeria Using Integrated Geophysical Methods. International Journal of Science and Techniques, 5 (5), 218 – 227.

[30] Eze, C.L., Sunday, V.N., Ugwu, S.A., Uko, E.D., Ngah, S.A. 2011. Mechanical model for Nigerian intraplate earth tremors. Earthzine. http://www.earthzine.org/2011/05/17/mechanical-model-for-nigerian-intraplate-earth-tremors

[31] Graham, K.M., Preko, K., Wemegah, D.D., Boamah, D. 2014. Geological and Structural Interpretation of part of the Buem Formation, Ghana, using Aero Geophysical Data. Journal of Environment and Earth Science, 4 (4), 17-31.

[32] Olujide, P.O., Udoh, A.N. 1989. Preliminary comments on the fracture systems of Nigeria. In: Proceedings of the national seminar on earthquakes in Nigeria, edited by Ajakaiye, D.E.; Ojo, S. B., Daniyan M. A. 97–109.